Energy & Environmental Science

Cite this: *Energy Environ. Sci.*, 2012, **5**, 6845

www.rsc.org/ees

COMMUNICATION

High-performance flexible lithium-ion electrodes based on robust network architecture†

Xilai Jia,‡[ab] Zheng Chen,‡[b] Arnold Suwarnasarn,[c] Lynn Rice,[b] Xiaolei Wang,[b] Hiesang Sohn,[b] Qiang Zhang,[a] Benjamin M. Wu,[c] Fei Wei*[a] and Yunfeng Lu*[b]

Received 7th November 2011, Accepted 31st January 2012
DOI: 10.1039/c2ee03110h

Highly robust, flexible, binder-free lithium-ion electrodes were fabricated based on interpenetrative nanocomposites of ultra-long CNTs and V_2O_5 nanowires. Such robust composite-network architecture provides the electrodes with effective charge transport and structural integrity, leading to high-performance flexible electrodes with high capacity, high rate-capability and excellent cycling stability.

Introduction

Flexible, lightweight energy-storage devices (batteries and supercapacitors) are of great interest for wearable devices, rollup displays, portable gadgets and other applications.[1,2] To convert such potentials into reality, one paramount challenge is the ability of making flexible electrodes with robust mechanical property and excellent electrochemical performance. To date, the most common approach for fabricating flexible electrodes is directly coating slurries containing electrode active materials, carbon and binder on flexible substrates such as plastic[1,3,4] or paper.[5,6] Such an approach, though, utilizes a substantial amount of inert components that inevitably compromise device energy density. As an alternative approach, flexible electrodes were fabricated from conducting polymers, such as polyaniline, polypyrrole and their derivatives;[7,8] however, such electrodes are brittle with low capacity (<150 mA h g^{-1}) and poor stability. Integrating conducting polymers with carbon nanotubes (CNTs)[9,10] or graphene[11] can improve the stability and flexibility but lead to decreased capacity.

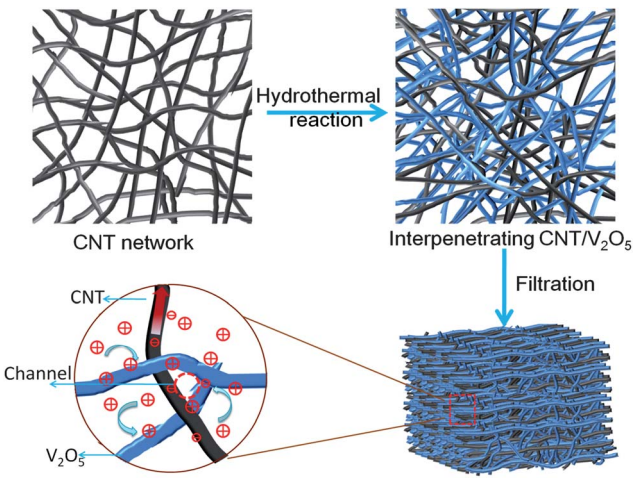

Fig. 1 Schematic of synthesis of the nanocomposites of ultra-long CNTs and V_2O_5 nanowires with an interpenetrative network structure.

[a]*Beijing Key Laboratory of Green Chemical Reaction Engineering and Technology, Department of Chemical Engineering, Tsinghua University, Beijing 100084, P. R. China. E-mail: wf-dce@tsinghua.edu.cn*
[b]*Department of Chemical and Biomolecular Engineering, University of California, Los Angeles, CA 90095, USA. E-mail: luucla@ucla.edu*
[c]*Department of Bioengineering, University of California, Los Angeles, CA 90095, USA*

† Electronic supplementary information (ESI) available: Fig. S1–S9. See DOI: 10.1039/c2ee03110h

‡ Both authors contributed to this work equally.

Broader context

Flexible, lightweight energy-storage devices are of great interest for wearable devices, rollup displays, portable gadgets and other applications. To realize the great potential, one paramount challenge is the ability of making flexible electrodes with robust mechanical property and excellent electrochemical performance. However, current approaches for fabricating high-performance flexible electrodes are still ineffective enough, which often leads to poor electrode performance. Herein, we demonstrate effective design and fabrication of highly robust, flexible, and binder-free lithium-ion electrodes based on interpenetrative nanocomposites of ultra-long CNTs and V_2O_5 nanowires. Such robust composite-network architecture enables effective charge transport and electrode integrity, thus endowing the electrodes with high capacity, high rate-capability and excellent cycling stability. This work provides a simple but effective strategy to fabricate flexible energy-storage devices.

Herein, we report a class of high-performance flexible electrodes based on composited networks of ultra-long CNTs and vanadium oxide (V_2O_5) nanowires, a high-energy material with a capacity of ~300 mA h g^{-1} based on two-lithium intercalation. As illustrated in Fig. 1, we started with networks of CNTs dispersed in a precursor solution of nanowires; an *in situ* hydrothermal reaction created three-dimensional (3-D) nanowire networks within the CNT networks, leading to the formation of CNT/nanowire composite gels with an interpenetrating network structure. Subsequent filtration condensed the networks into highly robust and flexible freestanding composite electrodes. Such a unique network structure provides critical features required for high-performance flexible electrodes: (i) the CNT scaffold provides fast electron transport pathways while the nanowire scaffold provides high charge-storage capacity with shortened lithium diffusion length; (ii) the network structure creates interconnected channels for effective ion transport; and (iii) the interpenetrating network of ultra-long CNTs and nanowires synergistically provides excellent mechanical robustness and high-rate lithium storage performance.

Note that flexible electrodes have been fabricated by depositing thin layers of V_2O_5 onto graphene paper with outstanding electrochemical performance; such electrodes, however, exhibit rather low capacity due to low V_2O_5 loading.[12] Similarly, flexible electrodes have been made from thin composites of In_2O_3 nanowires and CNTs but with extremely low In_2O_3 loading (<0.01 mg cm^{-2}).[13] Recently, flexible electrodes were reported by a simple physical mixing of CNTs with V_2O_5 nanowires; to achieve a moderate stability, the discharge cut-off potential was set to be rather high (*e.g.* 2.5 V *vs.* Li^+/Li),[14] leading to low capacity. Making V_2O_5 nanowire/graphene composites resulted in much improved capacity but unsatisfactory stability down to a low potential (1.5 V *vs.* Li^+/Li).[15] Strikingly, the robust mechanical property of such CNT/nanowire composites endows their corresponding bulk electrodes with high capacity, high rate and excellent stability down to a moderate potential (1.8 V *vs.* Li^+/Li). This work provides a simple but effective fabrication strategy towards making better flexible lithium-ion electrodes.

Experimental

Synthesis of the CNT/V_2O_5 composites

The ultra-long CNT arrays were prepared by the floating chemical vapor deposition (CVD) method.[16,17] Pristine CNTs were added into a cylinder by gas shearing to make ultra-long CNT aerogels.[18] Then the aerogels were immersed in 3 mol L^{-1} HCl solution to remove the residual catalyst impurities. The ultra-long CNTs were dried in a vacuum oven for 24 h at 120 °C. The structure of CNTs was characterized by scanning electron microscope (SEM) and transmission electron microscopy (TEM), as shown in Fig. S1†. An *in situ* hydrothermal method was used to synthesize the composites as described previously.[19] Briefly, appropriate amounts of the ultra-long CNT aerogels, HCl (2 M, 0.5 mL), ammonium metavanadate (NH_4VO_3, 0.15 g), surfactant P123 ($EO_{20}PO_{70}EO_{20}$, where EO and PO are ethylene oxide and propylene oxide, respectively, 0.25 g) and 15 mL of de-ionized water were mixed and stirred for 24 h. Then, the mixtures were transferred to 20 mL Teflon-lined autoclaves, heated to 120 °C and kept for 24 h in an oven. The resulting precipitates were filtered and washed with water and acetone several times then dried under vacuum at 120 °C for 24 h. The amounts of CNTs in the precursors were adjusted to 0.006, 0.020, 0.037, 0.005 and 0.075 g to obtain nanocomposites with CNT contents of 6, 15, 25, 30 and 40 wt %, respectively. CNT/V_2O_5 nanowire composites were also made using short CNTs with acid treatment.[19] Pure V_2O_5 nanowires were synthesized under the same conditions without adding CNTs.

Material and electrode characterizations

X-Ray diffraction was conducted on a Panalytical X'Pert Pro X-ray powder diffractometer using Cu-K_α radiation (λ = 1.54 Å). Nitrogen sorption isotherms were measured at 77 K with a Micromeritics ASAP 2020 analyzer. The specific surface areas (S_{BET}) were calculated by the Brunauer–Emmett–Teller (BET) method using an adsorption branch in a relative pressure range from 0.04 to 0.25. The pore size distributions (D_p) were derived from the adsorption branch of isotherms using the Barrett–Joyner–Halenda (BJH) model. SEM experiments were conducted on a JEOL JSM-6700 FE-SEM. TEM experiments were conducted on a Philips CM120 instrument operated at 120 kV. Mechanical tests were conducted on an INSTRON 5564 with a speed of 2.0 mm min^{-1} at room temperature. Details of the mechanical tests are provided as ESI (Fig. S2†). For the electrochemical test, the free-standing composite films were cut into desired sizes to make electrodes. The electrolyte solution was a 1 M $LiClO_4$ in propylene carbonate (PC) and lithium foils were used as both the counter and reference electrodes. The CV and EIS measurements were carried out on a Solartron 1860/1287 Electrochemical Interface. To make 2032-type coin cells, glass fiber (GF/D) papers from Whatman were used as the separators. Both the three-electrode cell test and coin cell assembly were conducted in an argon-filled glove box. The galvanostatic charge/discharge measurements were carried out by a LAND CT2000 battery tester at different rates.

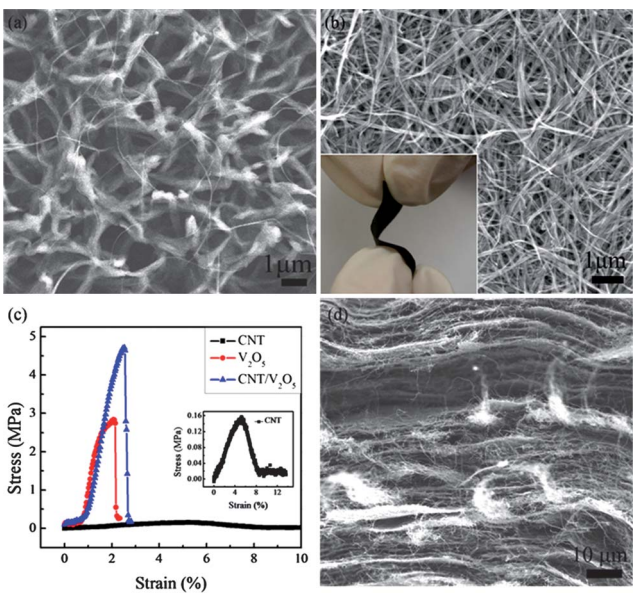

Fig. 2 (a) SEM image of V_2O_5 nanowire networks and CNTs penetrating through the networks. (b) SEM image of an electrode surface and a digital photograph of a flexible electrode with a dimension of 1 cm × 3 cm × 130 μm (inset). (c) Stress–strain curves of free-standing electrodes of CNTs, pure V_2O_5 nanowires, and CNT/V_2O_5 composites. (d) Cross-sectional SEM image of the CNT/V_2O_5 composite electrode.

Results and discussion

Fig. 2a shows a representative SEM image of a nanocomposite gel (25 wt% of CNTs), exhibiting a uniform nanowire network. Ultra-long CNTs are clearly observed interpenetrating through the nanowire network. The nanowires with diameters of 30–50 nm branch out and form a 3-D network structure. Microscopically, each nanowire has an ordered layered structure as evidenced from the selective area electron diffraction (SAED) (Fig. S3†) and X-ray diffraction patterns (Fig. S4†). Fig. 2b shows a digital photograph (inset) and SEM image of a flexible electrode with a fibrous network structure. Such a composite network structure creates interconnected pores and has a surface area of ~80 $m^2 g^{-1}$ and a broad pore size distribution from 6–30 nm (Fig. S5†).

Such a unique network structure endows the flexible electrodes with excellent mechanical robustness. Fig. 2c compares the stress–strain curves of electrodes based on nanowires, CNTs, and CNT/nanowire composites. As expected, the nanowire electrode is brittle with a breaking strain of 2.1% and strength of 2.8 MPa. The CNT electrode, on the other hand, shows a much lower strength of 0.16 MPa but a larger strain of 8.0%. The CNT/nanowire composite electrode shows a strength of 4.7 MPa, which is significantly higher than that of CNT and nanowire electrodes. The breaking strain of the composite electrode (2.8%) is only slightly higher than that of the nanowire electrode. The toughness of the nanocomposite (5.1×10^4 J m^{-3}), though, is almost twice that of the pure nanowire electrode (2.9×10^4 J m^{-3}) (Fig. S2†). Accordingly, the nanocomposite possesses an average modulus of 290 MPa, close to that of commercial paper. By comparison, flexible electrodes reported so far are still not strong enough to endure mechanical testing. To our knowledge, the strength of our nanocomposites exceeds that of all the other free-standing flexible electrodes and approaches that of many CNT sheets.[20]

Fig. 2d shows a cross-sectional SEM image of the ruptured surface of the nanocomposite electrode, revealing a unique multilayered structure. It was also found that the CNTs and nanowires are interconnected within these layers, which were stretched out from their entangled networks during the mechanical testing. Remarkably, removing V_2O_5 nanowires from the composite films using 37 wt% HCl resulted in CNT sheets that maintained the network integrity (Fig. S6†). We believe that the significantly enhanced mechanical performance of the composite electrodes is attributed synergistically to the interpenetrating structure between the ultra-long CNTs and V_2O_5 nanowires, which helps to absorb energy and accommodate mechanical stress during stretching.[21] The formation of a layered structure may be ascribed to the high aspect ratio of ultra-long CNTs, which are readily aligned during vacuum filtration.[20] In contrast, nanocomposites made from short CNTs do not show such a layered structure (Fig. S7†). We expect that the mechanical performance of the nanocomposites can be further enhanced by tuning CNT/nanowire compositions as well as their interface. Systematic studies to further improve mechanical performance are underway.

The robust structure endows CNT/V_2O_5 nanocomposite electrodes with excellent lithium storage capability, which was examined using various electrochemical tests. Cyclic voltammetry (CV) was first conducted to investigate their lithium storage behavior. In these studies, three-electrode cells using 1 M $LiClO_4$ in a propylene carbonate (PC) electrolyte were used. The voltage window was 1.8 to 4.0 V (*vs.* Li/Li^+). V_2O_5 nanowires present a typical layered structure

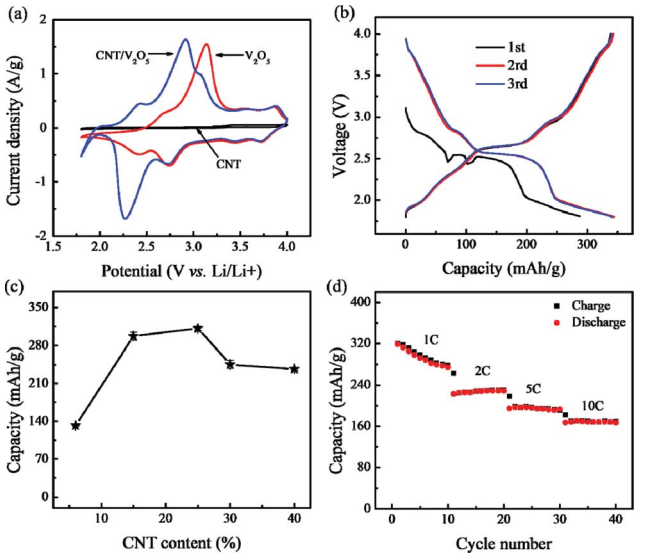

Fig. 3 (a) CV curves of CNT, V_2O_5, and CNT/V_2O_5 electrodes at a voltage range of 1.8 to 4 V (*vs.* Li/Li^+) at a potential scan rate of 1.0 mV s^{-1}. (b) First three charge/discharge cycles of a CNT/V_2O_5 nanocomposite electrode (containing 25 wt% CNTs) with a thickness of ~30 μm. (c) Dependence of lithium-storage capacity on the CNT content in composites. The current density was 70 mA g^{-1} and the capacity was calculated based on the mass of whole electrode. (d) Rate performance of the CNT/V_2O_5 cathode.

that can host a large amount of lithium ions. During the discharge process, which is accompanied by an electrochemical reduction, lithium ions are inserted mainly within the layers. While the charge process involves an electrochemical oxidation and lithium-ion extraction. More specifically, such electrochemical Li^+ insertion/extraction occurring can be expressed as $V_2O_5 + xLi^+ + xe^- \leftrightarrow Li_xV_2O_5$, where x is the mole fraction of inserted lithium ions. Fig. 3a compares the CV curves of a pure V_2O_5 nanowire electrode, a pure ultra-long CNT electrode, and a CNT/V_2O_5 (containing 25 wt% CNTs) nanocomposite electrode. The V_2O_5 nanowire electrode shows a pair of broad, asymmetric redox peaks, especially for the cathodic scan, indicating sluggish lithium ion insertion/extraction kinetics. In contrast, the nanocomposite electrode shows two pairs of well-defined redox peaks. The cathodic peaks at 2.3 and 2.7 V represent the lithium insertion from two different energy sites and correspond to the lithium extraction at 2.4 and 2.9 V by the anodic process, respectively, suggesting reversible charge/discharge processes. The improved electrode kinetics in the nanocomposite electrode is associated with improved transport in the hierarchical porous structure of the electrodes and, more importantly, increased conductivity due to the presence of an ultra-long CNT network. The pure CNT electrode shows a featureless CV curve with low capacitance due to the nature of electrical double layer capacitance; therefore, the capacitive contribution of CNTs within the composite electrode is relatively small compared to that of the nanowires.

To further quantify the lithium storage capability, galvanostatic charge/discharge was conducted using coin-cells where lithium discs were used as the negative electrodes. Fig. 3b shows the charge/discharge profiles of the CNT/V_2O_5 electrodes (25 wt% CNTs) at a current density of 70 mA g^{-1} between 1.8 and 4.0 V (*vs.* Li/Li^+). The lithium insertion during the first cycle is different from those observed in subsequent cycles due to the initial complex formation process.

From the second cycle, however, the charge/discharge process becomes stable. Three obvious plateaus at 3.8, 2.8, and 2.5 V are observed in the discharge curves, suggesting structure transition of V_2O_5 during the lithium-insertion process, which is similar to that of pure V_2O_5 electrodes and is consistent with previous reports.[22,23] The discharge capacity of the composite electrodes reaches up to 340 mA h g^{-1}, which exceeds that of the pure V_2O_5 nanowire electrodes (<100 mA h g^{-1}) and most nanostructured V_2O_5 electrodes reported so far.[14,22–27] Such an electrode still presents a capacity of over 260 mA h g^{-1} after 50 cycles at the charge/discharge rate of 0.25 C, suggesting good electrode stability (Fig. S8†).

To study the synergic effects between the conductive CNTs and high-capacity V_2O_5 nanowires, CNT/V_2O_5 composite electrodes (~30 μm thick) with various CNT compositions were examined. Fig. 3c shows their overall capacities *vs.* CNT content at a current density of 70 mA g^{-1}. The CNT/V_2O_5 electrodes with 6, 15, 25, 30 and 40 wt% loading of CNTs deliver reversible capacities of 130, 308, 318, 257 and 240 mA h g^{-1}, respectively. The composite electrodes with low CNT content (6 wt%) deliver low capacity due to inefficient electron transfer; alternatively, the composite electrodes with low V_2O_5 content (60 wt%) also show low capacity due to insufficient active material loading. A high discharge capacity is achieved at 25 wt % CNT loading, which is significantly higher than the sum of contributions from the CNT and nanowire constituents. A similar synergic effect was also observed in the aqueous electrolyte and other nanocomposite systems.[19,28]

Besides their high capacity, our robust composite electrodes also exhibit excellent rate-capability. Fig. 3d shows the rate performance of the composite electrode (25 wt% CNTs and with a thickness of ~30 μm). At a charge/discharge rate of 1 C (280 mA g^{-1}; 1 C corresponds to a full charge or discharge in 1 h), a capacity of 318 mA h g^{-1} is realized. At 2 C, though the capacity drops to 275 mA h g^{-1} after 10 cycles, it remains stable with a value of ~230 mA h g^{-1} thereafter. Even at very high rates, such as 5 C and 10 C, the electrode retains a capacity of 197 and 169 mA h g^{-1}, respectively. Note that such high rate performance has been achieved in thin film electrodes;[29] but has never been reported in such thick V_2O_5 electrodes. This excellent rate-capability is attributed to efficient electrolyte transport, fast lithium diffusion, and good electronic conductivity developed in the robust CNT/nanowire network.

Towards high-performance flexible devices, it is essential, but challenging, to make thick electrodes (>100 μm) with well-maintained capacity, rate-capability and cycling stability. The interpenetrating ultra-long CNT/nanowire network structure can realize this mission. Herein, CNT/V_2O_5 composite electrodes with 25 wt% CNTs and a thickness of ~130 μm were made and tested in coin-cells. As shown in Fig. 4a, the electrodes show a reversible capacity of ~280 mA h g^{-1} at a low rate of 0.5 C. Similar to thin electrodes, the capacity degrades slowly after 10 cycles at this rate. Nevertheless, after the initial drop, a reversible capacity of 120 mA h g^{-1} is achieved at 5 C with very slow capacity fading. Even after 200 cycles at 5 C, the electrode still maintains 87% (104 mA h g^{-1}) of its initial capacity at 5 C, suggesting an excellent stability during high-rate cycling. The Coulombic efficiency was only 92% at the first cycle, which is commonly observed for lithium-storage electrodes due to the irreversible replacement of protons and formation of some solid–electrolyte interface.[30–32] Nevertheless, the efficiency reached ~100% from the second cycle and was maintained at ~100% during the following cycles, suggesting a high reversibility. Note that, for V_2O_5-based

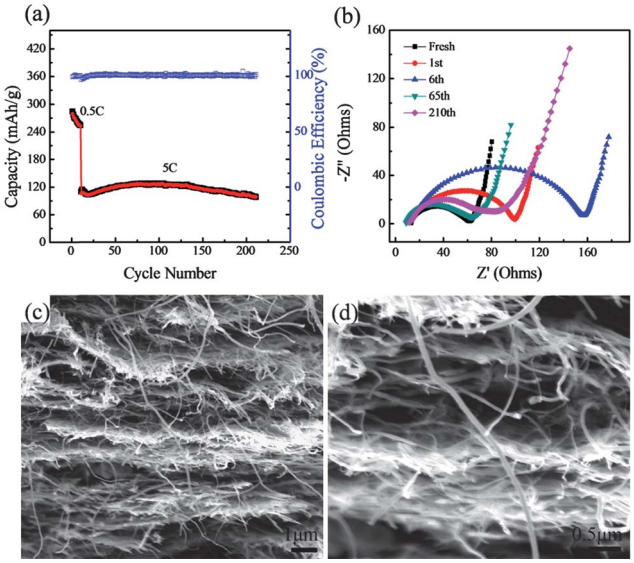

Fig. 4 (a) Cycling performance of a CNT/V_2O_5 electrode with 25 wt% CNTs and a thickness of ~130 μm. (b) Nyquist plots of the CNT/V_2O_5 electrode at different cycling stages. (c and d) Cross-sectional SEM images of the CNT/V_2O_5 electrode after 210 cycles.

lithium electrodes, a common issue is capacity fading due to the structure and volume changes, which often results in more than 20% of the capacity loss within 100 cycles.[14,22–27] These ultra-long-CNT based composites, though, show high mechanical strength and strain tolerance, consequently providing the electrodes with significantly enhanced cycling stability. In contrast, composites made by physically mixing V_2O_5 nanowires with short CNTs have much lower capacity and poor cycling stability.[14,15] Based on these studies, it is reasonable to conclude that mechanical robustness is essential for ensuring electrode cycling stability.

To further understand the structure and interface stability of our nanocomposite electrodes during cycling, electrochemical impedance spectroscopy (EIS) was conducted along with galvanostatic charge/discharge (Fig. 4b). The Nyquist plots exhibit a single semicircle at high frequency, which is due to a combination of a resistance, capacitance, and constant phase element of the electrode. The ohmic resistance of the electrode is nearly constant during cycling, indicating good contact between the current collector and the electrode, as well as structure integrity of the electrode. The charge transfer resistance (diameter of the semicircle) increases from 50 Ω to 150 Ω after 6 initial cycles due to solid–electrolyte-interface (SEI) formation and proton replacement during initial cycles.[30–32] This causes some irreversibility and capacity fading, agreeing well with the charge/discharge results. Very interestingly, the internal resistance of the electrode decreases to its initial value after 65 cycles, whereafter the charge/discharge capacity increases, which suggests that the CNT/nanowire network structure forms a robust and stable electrode. The decreased electrode resistance after 6 cycles may be due to removal of the protons from the electrodes and a better CNT–V_2O_5 interface induced by the charge/discharge process. In the following cycles, the resistance is relatively stable and accordingly, electrode capacity was well maintained. To further confirm the electrodes' structure integrity, the lithiated electrode (electrode discharged to 1.8 V) and the electrode cycled for 210 cycles were taken out of the coin-cells and examined under SEM. As shown in Fig. S9† and 4c and d, the electrodes

retained their initial multilayered structure with an interpenetrating network, further confirming the mechanical robustness.

Conclusions

In summary, we have demonstrated an efficient synthesis of highly robust, flexible, binder-free electrodes based on interpenetrative nanocomposites of V_2O_5 nanowires and ultra-long CNTs. Such robust network architecture enables effective charge transport and electrode integrity, endowing the electrodes with high capacity, high rate-capability and excellent cycling stability for high-performance flexible device applications.

Acknowledgements

This work was partially supported by the China National Program (2011CB932602) and the Center for Molecularly Assembled Material Architectures for Solar Energy Production, Storage and Carbon Capture, an Energy Frontier Research Center funded by the U.S. Department of Energy, Office of Science, and Office of Basic Energy Sciences under award DE-SC0001342.

Notes and references

1 H. Nishide and K. Oyaizu, *Science*, 2008, **319**, 737.
2 V. L. Pushparaj, M. M. Shaijumon, A. Kumar, S. Murugesan, L. Ci, R. Vajtai, R. J. Linhardt, O. Nalamasu and P. M. Ajayan, *Proc. Natl. Acad. Sci. U. S. A.*, 2007, **104**, 13574.
3 F. Meng and Y. Ding, *Adv. Mater.*, 2011, **23**, 4098.
4 B. G. Choi, J. Hong, W. H. Hong, P. T. Hammond and H. Park, *ACS Nano*, 2011, **5**, 7025.
5 L. Hu, J. W. Choi, Y. Yang, S. Jeong, F. La Mantia, L. Cui and Y. Cui, *Proc. Natl. Acad. Sci. U. S. A.*, 2009, **106**, 21490.
6 L. Hu, H. Wu, F. La Mantia, Y. Yang and Y. Cui, *ACS Nano*, 2010, **4**, 5843.
7 G. A. Snook, P. Kao and A. S. Best, *J. Power Sources*, 2011, **196**, 1.
8 L. Nyholm, G. Nyström, A. Mihranyan and M. Strømme, *Adv. Mater.*, 2011, **23**, 3751.
9 C. Meng, C. Liu, L. Chen, C. Hu and S. Fan, *Nano Lett.*, 2010, **10**, 4025.
10 C. Meng, C. Liu and S. Fan, *Electrochem. Commun.*, 2009, **11**, 186.
11 Q. Wu, Y. Xu, Z. Yao, A. Liu and G. Shi, *ACS Nano*, 2010, **4**, 1963.
12 H. Gwon, H. S. Kim, K. U. Lee, D. H. Seo, Y. C. Park, Y. S. Lee, B. T. Ahn and K. Kang, *Energy Environ. Sci.*, 2011, **4**, 1277.
13 P. Chen, G. Shen, S. Sukcharoenchoke and C. Zhou, *Appl. Phys. Lett.*, 2009, **94**, 043113.
14 K. H. Seng, J. Liu, Z. P. Guo, Z. X. Chen, D. Jia and H. K. Liu, *Electrochem. Commun.*, 2011, **13**, 383.
15 H. Liu and W. Yang, *Energy Environ. Sci.*, 2011, **4**, 4000.
16 Q. Zhang, W. Zhou, W. Qian, R. Xiang, J. Huang, D. Wang and F. Wei, *J. Phys. Chem. C*, 2007, **111**, 14638.
17 Q. Zhang, D. Wang, J. Huang, W. Zhou, G. Luo, W. Qian and F. Wei, *Carbon*, 2010, **48**, 2855.
18 Q. Zhang, G. Xu, J. Huang, W. Zhou, M. Zhao, Y. Wang, W. Qian and F. Wei, *Carbon*, 2009, **47**, 538.
19 Z. Chen, Y. Qin, D. Weng, Q. Xiao, Y. Peng, X. Wang, H. Li, F. Wei and Y. Lu, *Adv. Funct. Mater.*, 2009, **19**, 3420.
20 G. Xu, Q. Zhang, W. Zhou, J. Huang and F. Wei, *Appl. Phys. A: Mater. Sci. Process.*, 2008, **92**, 531.
21 Q. Zhang, M. Zhao, Y. Liu, A. Cao, W. Qian, Y. Lu and F. Wei, *Adv. Mater.*, 2009, **21**, 2876.
22 A. Cao, J. Hu, H. Liang and L. Wan, *Angew. Chem., Int. Ed.*, 2005, **44**, 4391.
23 Y. Hu, X. Liu, J. Müller, R. Schlögl, J. Maier and D. S. Su, *Angew. Chem., Int. Ed.*, 2009, **48**, 210.
24 P. Liu, S. H. Lee, C. E. Tracy, Y. Yan and J. A. Turner, *Adv. Mater.*, 2002, **14**, 27.
25 Y. Wang, K. Takahashi, K. H. Lee and G. Z. Cao, *Adv. Funct. Mater.*, 2006, **16**, 1133.
26 D. Liu, Y. Liu, A. Pan, K. P. Nagle, G. T. Seidler, Y. Jeong and G. Cao, *J. Phys. Chem. C*, 2011, **115**, 4959.
27 L. Mai, L. Xu, C. Han, X. Xu, Y. Luo, S. Zhao and Y. Zhao, *Nano Lett.*, 2010, **10**, 4750.
28 B. Guo, X. Wang, P. F. Fulvio, M. Chi, S. M. Mahurin, X.-G. Sun and S. Dai, *Adv. Mater.*, 2011, **23**, 4661.
29 Y. Liu, M. Clark, Q. Zhang, D. Yu, D. Liu, J. Liu and G. Cao, *Adv. Energy Mater.*, 2011, **1**, 194.
30 W. J. H. Borghols, D. Lützenkirchen-Hecht, U. Haake, W. Chan, U. Lafont, E. M. Kelder, E. R. H. van Eck, A. P. M. Kentgens, F. M. Mulder and M. Wagemaker, *J. Electrochem. Soc.*, 2010, **157**, A582.
31 Y. Chang, H. Li, L. Wu and T. Lu, *J. Power Sources*, 1997, **68**, 187.
32 G. Ning, B. Haran and B. N. Popov, *J. Power Sources*, 2003, **117**, 160.